

Article

Using Isotopic and Hydrochemical Indicators to Identify Sources of Sulfate in Karst Groundwater of the Niangziguan Spring Field, China

Chunlei Tang ^{1,2}, Hua Jin ^{1,*} and Yongping Liang ^{2,*}

¹ College of Water Resources Science and Engineering, Taiyuan University of Technology, Taiyuan 030024, China; yourfriendtcl@163.com

² Key Laboratory of Karst Dynamics, Ministry of Land and Resources, Institute of Karst Geology, Chinese Academy of Geological Sciences, Guilin 541004, China

* Correspondence: jinhua@tyut.edu.cn (H.J.); lyp0261@karst.ac.cn (Y.L.); Tel.: +86-136-4783-1258 (H.J.)

Abstract: Karst groundwater in the Niangziguan spring fields is the main source to supply domestic and industrial water demands in Yangquan City, China. However, the safety of water supply in this region has recently suffered from deteriorating quality levels. Therefore, identifying pollution sources and causes is crucial for maintaining a reliable water supply. In this study, a systematic sample collection for the karst groundwater in the Niangziguan spring fields was implemented to identify hydrochemical characteristics of the karst groundwater through comprehensive analyses of hydrochemistry (piper diagram, and ion ratios,) and stable isotopes (S and H-O). The results show that the karst groundwater in the Niangziguan spring fields was categorized as $\text{SO}_4\cdot\text{HCO}_3\text{-Ca}\cdot\text{Mg}$, $\text{HCO}_3\cdot\text{SO}_4\text{-Ca}\cdot\text{Mg}$, and $\text{SO}_4\text{-Ca}$ types. K^+ , Cl^- , and Na^+ are mainly sourced from urban sewage and coal mine drainage. In addition, SO_4^{2-} was mainly supplied by the dissolution of gypsum and the oxidation of FeS_2 in coal-bearing strata. It is noteworthy that, based on H-O and S isotopes, 75% of the karst groundwater was contaminated by acidic water in coal mines at different degrees. In the groundwater of the Niangziguan spring field, the proportions of SO_4^{2-} derived from FeS_2 oxidation were 60.6% (N50, Chengxi spring), 30.3% (N51, Wulong spring), and 26.0% (N52, Four springs mixed with water). Acid mine drainage directly recharges and pollutes karst groundwater through faults or abandoned boreholes, or discharges to rivers, and indirectly pollutes karst groundwater through river infiltration in carbonate exposed areas. The main source of rapid increase of sulfate in karst groundwater is acid water from abandoned coal mines.



Citation: Tang, C.; Jin, H.; Liang, Y. Using Isotopic and Hydrochemical Indicators to Identify Sources of Sulfate in Karst Groundwater of the Niangziguan Spring Field, China. *Water* **2021**, *13*, 390. <https://doi.org/10.3390/w13030390>

Academic Editor:

Alexander Yakirevich

Received: 16 December 2020

Accepted: 29 January 2021

Published: 3 February 2021

Keywords: karst spring; hydrochemical characteristics; source of sulfate; stable isotope

Publisher's Note: MDPI stays neutral with regard to jurisdictional claims in published maps and institutional affiliations.



Copyright: © 2021 by the authors. Licensee MDPI, Basel, Switzerland. This article is an open access article distributed under the terms and conditions of the Creative Commons Attribution (CC BY) license (<https://creativecommons.org/licenses/by/4.0/>).

1. Introduction

Karst regions occupy approximately 25 percent of the land surface of the Earth [1–3]. Karst groundwater is an important water resource that is used as a drinking and industrial water source by a significant proportion of the world's population [4,5]. However, karst aquifers are much more vulnerable to pollution than other aquifers, and the restoration of contaminated groundwater is difficult [6–8]. Karst groundwater is a “hidden resource” in northern China and the prevention and monitoring of karst groundwater pollution are more difficult than that of surface waters due to its inaccessibility. Among numerous contaminants that contribute to groundwater pollution, Fe [9–12], nitrate [13–17], and sulfate [18–20] are cited most frequently. Fe in karst groundwater is mainly affected by Fe-rich acid mine drainage (AMD). Nitrate in karst groundwater includes synthetic and organic fertilizers, as well as municipal and industrial sewage. Sulfate minerals in karst groundwater originate from natural sources like the dissolution of sulfate, atmospheric deposition, and AMD caused by human activity.

Niangziguan spring is located in Yangquan City, Shanxi Province. The average annual flow of spring water is $9.8 \text{ m}^3\cdot\text{s}^{-1}$ (1956–2019). Spring water in the Niangziguan spring

fields is the main source to supply domestic and industrial water demands in Yangquan City, China. Since 2010, the sulfate radical of karst spring water has been more than $250 \text{ mg}\cdot\text{L}^{-1}$. Karst well water and springs are the primary method used for the discharge of groundwater from karst aquifers [21,22]. Therefore, the monitoring of karst well water and springs can provide more insights into the hydrogeological and hydrogeochemical processes that occur in underground environments.

The hydrogeochemical characteristics are crucial to reflect the circulation and hydrodynamic conditions of regional groundwater, and to understand the water quality and distribution characteristics. To date, methods commonly used in the karst water hydrogeochemistry are the hydrochemical type, saturation index, and ion ratio methods [23–25]. Advanced techniques have been also used such as isotopic analysis, statistical methods, and hydrogeochemical simulations. The interactions between precipitation and groundwater can be investigated using stable isotopes of hydrogen and oxygen [26–29]. The application of isotope tracers ($\delta^{34}\text{S}\text{-SO}_4^{2-}$, $\delta^{18}\text{O}\text{-SO}_4^{2-}$) in identifying sources and fate of SO_4 in groundwater has been successfully achieved for several decades [30–35]. The geochemical evolution of karst water and its associations with urbanization impacts have not been fully addressed in the karst regions throughout the world [36–42]. This study characterizes spatial-temporal variations in hydrochemistry in the Niangziguan spring region, a typical karst area of fast urbanization in Shanxi, using hydrochemical reconnaissance and monitoring of S, D, and O isotopes [43–49]. The aim of our study is to evaluate the impacts of rapid urbanization on karst water quality. Identifying pollution sources and causes is crucial for reliable water supply.

2. Materials and Methods

2.1. Study Area

The Niangziguan spring field is located in the eastern part of Shanxi Province adjacent to Hebei Province in China, which includes: (1) the urban areas, suburbs, Pingding County, and Yu County of Yangquan City; (2) Xiyang, Heshun, Zuoquan, Shouyang, and Yuci of Jinzhong City; (3) Taiyuan City and Yangqu County. These areas are shown in Figure 1. The distribution area of coal measures strata in the spring area is 4728 km^2 , accounting for 63.5% of the whole spring area. Therefore, the industrial structure dominated by coal has become a feature of this area. Taking a comprehensive view of the main districts and counties in the spring area (the districts and counties of Yangquan City and Shouyang, Xiyang, Heshun, and Zuoquan of Jinzhong City), the output value of coal mining industry generally accounts for more than 50% of the total output value. The total area of the district is 7436 km^2 ranging from $36^\circ 55' \text{ N}$ to $38^\circ 15' \text{ N}$ and $112^\circ 20' \text{ E}$ to $113^\circ 55' \text{ E}$. The average annual water evaporation in the study area was 1202 mm while the average annual precipitation of the whole region was 542.4 mm during the period from 1955 to 2019 at Yangquan Station within the China Meteorological Data Network. While the average annual temperature is $10.9 \text{ }^\circ\text{C}$, the average temperature in January is $-4.6 \text{ }^\circ\text{C}$ and the extreme minimum temperature is $-28 \text{ }^\circ\text{C}$.

2.2. Materials and Methods

Fifty-two karst well water or springs in the Niangziguan spring field were sampled during 23–24 June 2014 and analyzed for constant indicators (water temperature, pH, conductivity, Ca^{2+} , Mg^{2+} , K^+ , Na^+ , Cl^- , SO_4^{2-} , HCO_3^- , NO_3^- , CO_3^{2-} , etc.) and trace indicators (Sr^{2+} , F^-). With 18 groups of acidic drainage and surface water samples collected from coal mines in the spring field in April 2013, June 2014, October 2015, and April 2019, the constant indicators (water temperature, pH, conductivity, Ca^{2+} , Mg^{2+} , K^+ , Na^+ , Cl^- , SO_4^{2-} , HCO_3^- , CO_3^{2-} , etc.) and isotope ($\delta^{34}\text{S}$) were measured. The temperature, pH, conductivity (EC), and ORP were directly measured by a WTW 3440 (Xylem Analytics, Munich, Germany) water quality parameter tester in the field. Ca^{2+} and HCO_3^- were titrated in the field by the Merck test box (MColorTest™ 1.11110.0001, Germany), with a measurement accuracy of $1 \text{ mg}\cdot\text{L}^{-1}$ and $0.1 \text{ mmol}\cdot\text{L}^{-1}$, respectively.

The concentrations of Mg^{2+} , K^+ , Na^+ , and Sr^{2+} were measured with ICP-AES (ICAP 7600, Thermo Fisher, Waltham, MA USA). SO_4^{2-} , HCO_3^- , NO_3^- , CO_3^{2-} , and F^- were analyzed with ion chromatography (Dionex ICS-1100, Thermo Fisher, USA). The detection limits were $0.02\text{ mg}\cdot\text{L}^{-1}$, $0.06\text{ mg}\cdot\text{L}^{-1}$, $0.008\text{ mg}\cdot\text{L}^{-1}$, $0.03\text{ mg}\cdot\text{L}^{-1}$, $0.01\text{ mg}\cdot\text{L}^{-1}$, $0.01\text{ mg}\cdot\text{L}^{-1}$, $0.01\text{ mg}\cdot\text{L}^{-1}$, $0.01\text{ mg}\cdot\text{L}^{-1}$, and $0.02\text{ mg}\cdot\text{L}^{-1}$ for Mg^{2+} , K^+ , Na^+ , Sr^{2+} , SO_4^{2-} , HCO_3^- , NO_3^- , CO_3^{2-} , and F^- , respectively. δD_{H_2O} and $\delta^{18}O_{H_2O}$ isotopes were determined using a stable isotope ratio mass spectrometer (IRMS, MAT253, Thermo Fisher, USA). Detection of major ions, trace elements, δD_{H_2O} , and $\delta^{18}O_{H_2O}$ were performed at the Karst Geological Resources and Environment Supervision and Monitoring Centre of the Ministry of Land and Resources. Stable sulfur of dissolved sulfates was measured at the China University of Geosciences (Wuhan) using a stable IRMS (Delta V advantage, Thermo Fisher Scientific, USA). The stable Hydrogen and Oxygen data of water are expressed in delta (δ) as parts per thousand (‰) relative to the Vienna Standard Mean Ocean Water (V-SMOW). Stable sulfur data of dissolved sulfates are expressed in delta (δ) as parts per thousand (‰) relative to the Vienna Canyon Diablo Troilite (V-CDT).

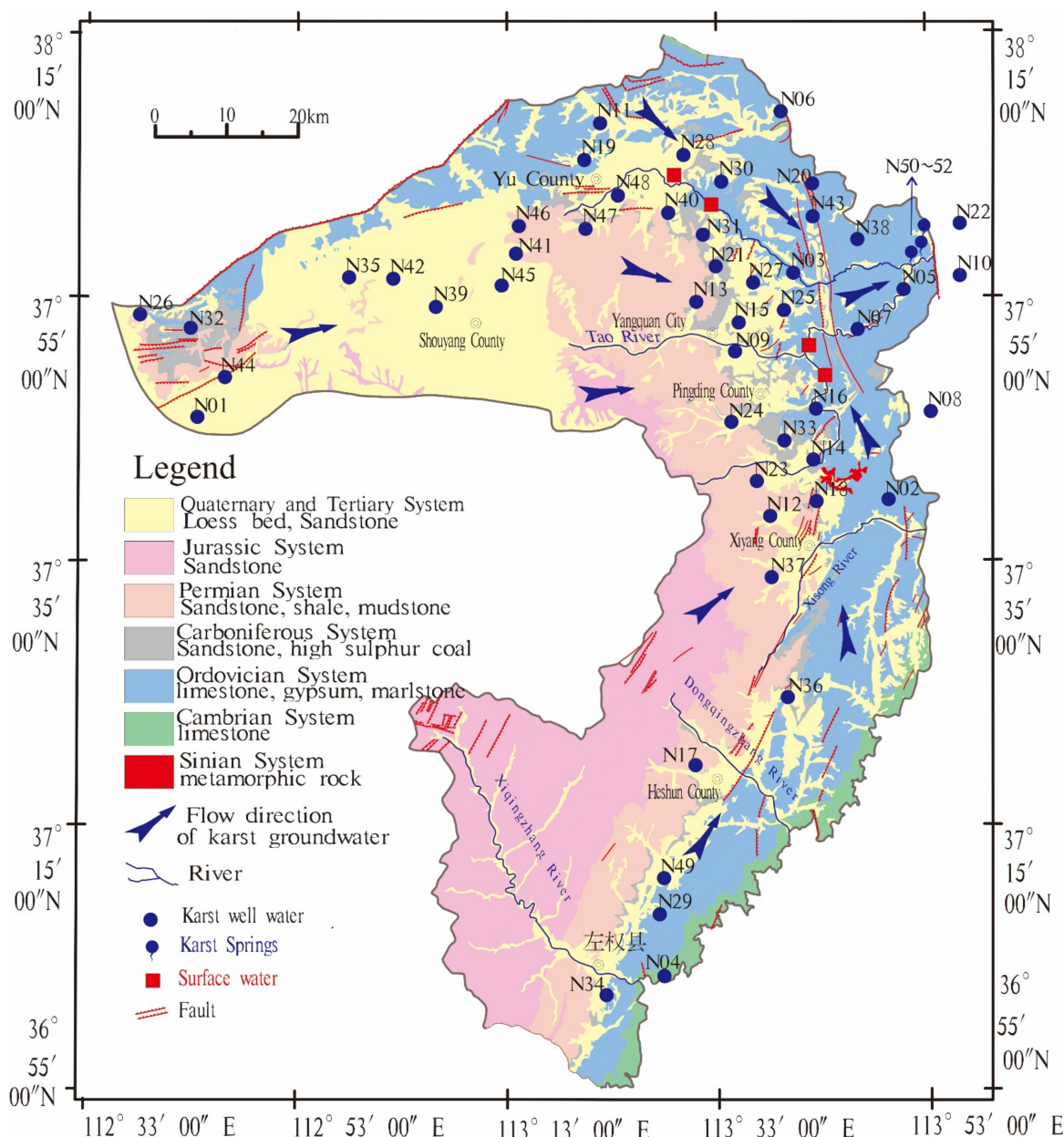


Figure 1. Hydrogeological map of Niangziguan spring catchment.

3. Results and Discussion

3.1. Hydrogeochemistry

The chemical composition of karst water is controlled by factors such as geological conditions, hydrodynamic conditions, and human engineering activities in the region, and it can better preserve such influence information [50–54]. Therefore, hydrogeologists often use hydrogeochemical methods to study complex karst water systems [55–58].

3.1.1. Hydrogeochemistry of the Karst Groundwater

Based on a total of 52 sets of analytical results for the karst groundwater, it was found that the pH values of karst water range from 6.96 to 8.00, with an average of 7.60. The average concentrations of Ca^{2+} , Mg^{2+} , $\text{K}^+\text{+Na}^+$, Cl^- , and SO_4^{2-} are $143.5 \text{ mg}\cdot\text{L}^{-1}$, $36.2 \text{ mg}\cdot\text{L}^{-1}$, $45.6 \text{ mg}\cdot\text{L}^{-1}$, and $323.9 \text{ mg}\cdot\text{L}^{-1}$, respectively. The ranges of each indicator are shown in Table 1 and Figure 2. Figure 3 shows a piper diagram of ionic concentration for the collected samples. The karst water (spring) generally shows cationic high concentrations of Ca^{2+} and Mg^{2+} and low concentrations of $\text{K}^+\text{+Na}^+$, and anionic high concentration of SO_4^{2-} , low concentrations of Cl^- , and high concentration of HCO_3^- (Table 1).

Table 1. Statistical summary of water quality parameters and stable isotopes in karst groundwater.

Sample NO.	Type	T/°C	pH	Major Elements (mg·L ⁻¹)								‰		
				Ca ²⁺	Mg ²⁺	K ⁺	Na ⁺	Cl ⁻	SO ₄ ²⁻	HCO ₃ ⁻	CO ₃ ⁻	D	¹⁸ O	³⁴ S
N01	karst well	20	7.8	100.9	34.1	1.36	62.9	19.5	304.2	212.5	n.d.	-70	-9.3	-6.11
N02	karst well	21	7.55	120	19.3	2.52	22.1	17.7	221.2	188.2	n.d.	-49	-5.8	-3.54
N03	karst well	16	7.7	329.1	68.5	4.23	131.4	70.9	1029	176.1	n.d.	-63	-8.5	-0.21
N04	karst well	15	7.7	126.2	21.2	2.32	65.7	36.5	231.6	248.9	n.d.	-65	-8.5	0.77
N05	karst well	18	7.21	223.4	48.5	6.56	193.6	164.9	623.5	273.2	n.d.	-60	-8	4.03
N06	karst well	14	7.8	87.8	16.5	0.75	46.4	14.2	106	261.1	n.d.	-69	-9.4	4.24
N07	karst well	19.9	7.53	220.3	44.3	5.45	149.5	152.5	536.2	261.1	n.d.	-62	-8.2	4.84
N08	karst well	14.5	7.8	71.5	15.3	0.75	33.3	12.4	104	191.2	n.d.	-68	-9.2	4.97
N09	karst well	16	7.5	183.9	37.5	3.43	99.8	86.9	427	261.1	n.d.	-63	-8.4	5.98
N10	karst well	19.2	7.8	67.4	18.2	1.05	33.2	16	97.1	200.4	n.d.	-68	-9.4	6.14
N11	karst well	17.5	7.5	77.9	23.9	1.04	10.6	6	21.7	303.6	n.d.	-69	-9.3	6.37
N12	karst well	17.1	7.9	98.2	27.2	1.38	12.6	16.7	118.4	245.9	n.d.	-70	-9.5	7.22
N13	karst well	18	7.5	329.9	79.1	3.45	125.2	65.6	975.2	297.5	n.d.	-67	-8.9	7.43
N14	karst well	19.2	7.5	69.5	30.9	1.3	48.4	8.9	202	206.4	n.d.	-70	-9.4	7.49
N15	karst well	15.9	7.14	262.6	55.6	3.16	78.3	101	595.1	297.5	n.d.	-63	-8.5	8.56
N16	karst well	25.8	8	220.7	46.5	5.01	115.6	119.5	664.6	112.3	n.d.	-52	-6.2	9.41
N17	karst well	17	7.57	185.3	40.1	1.2	10.4	9.6	357.8	270.8	n.d.	-73	-10	10.31
N18	karst well	17	7.86	96.4	24.9	1.26	10.4	16	112.5	230.7	n.d.	-70	-9.4	10.43
N19	karst well	17	7.6	66.8	21.3	0.76	50.4	13.1	111.5	236.8	n.d.	-71	-9.7	11.86
N20	karst well	19	7.6	78.8	23.1	1.28	6.3	9.6	41.7	276.2	n.d.	-71	-9.8	12.24
N21	karst well	20.7	7.87	164.3	46.5	2.18	50.4	58.5	396.9	212.5	n.d.	-71	-9.6	12.31
N22	karst well	19.4	7.8	141.4	39.2	2.89	74.4	69.1	320.3	242.9	n.d.	-69	-9.2	13.55
N23	karst well	19.7	7.8	81.4	28.3	1.12	35	12.4	175.7	203.4	n.d.	-70	-9.5	14.1
N24	karst well	15	7.7	133.7	36.5	1.09	35.2	21.6	286.6	224.6	n.d.	-67	-8.9	14.6
N25	karst well	17	8	84.8	25.5	1.26	40.1	23.8	177.6	194.3	n.d.	-65	-8.5	14.66
N26	karst well	16	7.5	62.1	22.1	0.82	10.1	7.1	24.4	264.1	n.d.	-72	-10	15.12
N27	karst well	19.4	7.5	207.9	52.2	1.27	22	26.6	495.6	227.7	n.d.	-68	-9.3	16.45
N28	karst well	15.8	7.8	72.5	20.3	1.07	51.2	7.1	117.3	267.1	n.d.	-70	-9.5	16.87
N29	karst well	17.5	7.7	89.9	21.2	1.27	40.9	12.4	147.5	236.8	n.d.	-68	-9.2	17
N30	karst well	17	7.75	66.7	24.4	1.06	6.7	6	29.1	276.2	n.d.	-73	-9.9	17.02
N31	karst well	20.5	6.96	375.8	71.9	1.75	20.4	30.1	1043	236.8	n.d.	-67	-9	17.3
N32	karst well	20	7.5	68.4	24.8	0.95	13	8.9	64.2	255	n.d.	-72	-9.9	17.46
N33	karst well	17	7.5	125	40.5	1.15	35.5	12.4	320.8	218.6	n.d.	-68	-9.1	17.98
N34	karst well	17	7.8	115.8	28.7	0.97	36.5	9.2	252.8	225.9	n.d.	-74	-9.6	18.03
N35	karst well	17	7.5	99.6	36.4	1.38	13.1	8.9	193.6	239.8	n.d.	-73	-10.1	19.08
N36	karst well	16.1	7.6	112.4	27.9	0.95	8	12.4	139.5	267.1	n.d.	-74	-10.1	19.16
N37	karst well	18.1	7.5	119.5	30	1.09	8.3	7.1	176.6	261.1	n.d.	-72	-9.9	20.52
N38	karst well	17.6	8	141.5	34.2	4.99	35.6	47.9	349.8	145.7	n.d.	-69	-9.4	21.15

Table 1. Cont.

Sample NO.	Type	T/°C	pH	Major Elements (mg·L ⁻¹)								‰		
				Ca ²⁺	Mg ²⁺	K ⁺	Na ⁺	Cl ⁻	SO ₄ ²⁻	HCO ₃ ⁻	CO ₃ ⁻	D	¹⁸ O	³⁴ S
N39	karst well	17	7.3	127.5	42.3	1.46	14.2	8.9	293.7	242.9	n.d	-73	-10.1	21.18
N40	karst well	20.7	7.18	346.6	65.9	1.32	16.8	12.4	916.5	252	n.d	-70	-9.7	22.06
N41	karst well	19	7.4	132.2	41	0.86	13.2	9.6	257.7	256.2	n.d	-72	-9.7	22.6
N42	karst well	20	7.6	112.6	36.9	1.2	12.4	7.1	272.6	206.4	n.d	-73	-10	22.65
N43	karst well	22	7.8	119.7	24.9	0.94	9.7	16	236.2	145.7	n.d	-66	-8.9	24.47
N44	karst well	19	7.4	115	31.8	1.26	12.6	8.9	222	224.6	n.d	-74	-10.1	24.52
N45	karst well	25.9	7.7	100.2	32.8	0.99	11.3	7.1	181.6	236.8	n.d	-73	-10.1	24.62
N46	karst well	20.5	7.86	122.9	51.3	0.94	10.7	8.9	307.4	245.9	n.d	-71	-9.7	24.87
N47	karst well	20.8	7.26	334	70.5	1.3	46.8	16	918.3	276.2	n.d	-70	-9.5	24.97
N48	karst well	19	7.6	160	35.4	1.24	46	7.8	386.4	236.8	n.d	-71	-9.6	26.06
N49	karst well	20.9	7.3	166.8	38.5	1.53	51	9.6	431.7	233.7	n.d	-70	-9.3	27.68
N50	Chengxi spring	16	7.6	118.4	31.6	2.05	42.8	53.2	185.3	255	n.d	-68	-9.1	8.31
N51	Wulong spring	19	7.66	127.2	35.6	1.92	71.1	58.5	315.1	233.7	n.d	-71	-9.6	17.26
N52	Jiquanzhan	19	7.45	101.8	36	2.03	74.4	60.3	326.9	157.9	n.d	-71	-9.7	18.54

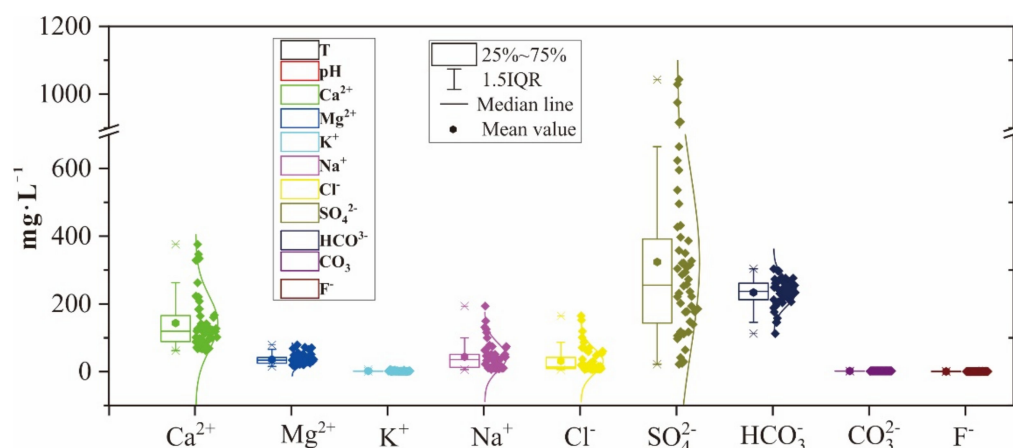


Figure 2. Box chart of ionic concentration in karst groundwater of Niangziguan spring catchment.

The results show that the karst groundwater in Niangziguan Spring area can be divided into three types: SO₄·HCO₃-Ca·Mg, HCO₃-SO₄-Ca·Mg, and SO₄-Ca types. The sulfate content in 51.9% of the karst groundwater samples exceeds the standard (Standards for drinking water quality, GB 5749-2006 in China).

3.1.2. Hydrogeochemistry of Acidic Mine Drainage (AMD) and Surface Water (River)

Figure 4 shows pH values ranging from 2.75 to 7.48 (an average of 5.41). The concentrations of Ca²⁺, Mg²⁺, K⁺+Na⁺, Cl⁻, and SO₄²⁻ were 246.4 to 676.1 mg·L⁻¹ (an average of 505.6 mg·L⁻¹), 69.1–1119.8 mg·L⁻¹ (an average of 391.5 mg·L⁻¹), 23.8–686.8 mg·L⁻¹ (an average of 167.2 mg·L⁻¹), 3.1–144.0 mg·L⁻¹ (average of 45.4 mg·L⁻¹), and 1138–16218 mg·L⁻¹ (an average of 5119.2 mg·L⁻¹), respectively. As shown in Figure 5, the concentrations of Cl⁻ and SO₄²⁻ ranged from 14.2 to 522.9 mg·L⁻¹ (an average of 136.1 mg·L⁻¹) and 183.2 to 4042 mg·L⁻¹ (an average of 1240.7 mg·L⁻¹), respectively. These results are closely related to the Shukarev classification types for the coal mine acidic water and surface water. In other words, the coal mine acidic water is usually grouped by SO₄-Ca·Mg and SO₄-Mg·Ca types while the surface water is mainly classified by SO₄-Ca·Na and SO₄-Ca types. Therefore, the coal mine acidic water generally exhibited high concentrations of Ca²⁺, Mg²⁺, and SO₄²⁻ while the surface water showed a higher concentration of Cl⁻ than that of the acidic water from coal mines (Figure 6).

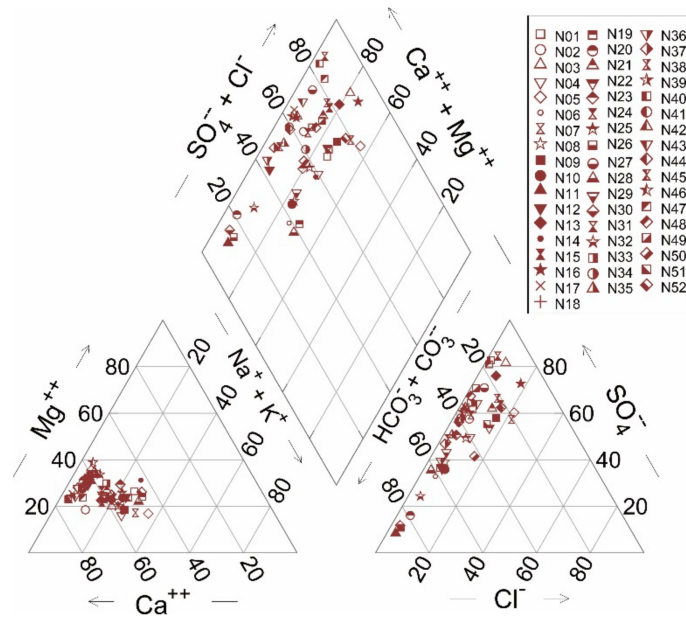


Figure 3. Piper diagram of ionic concentrations in the karst groundwater.

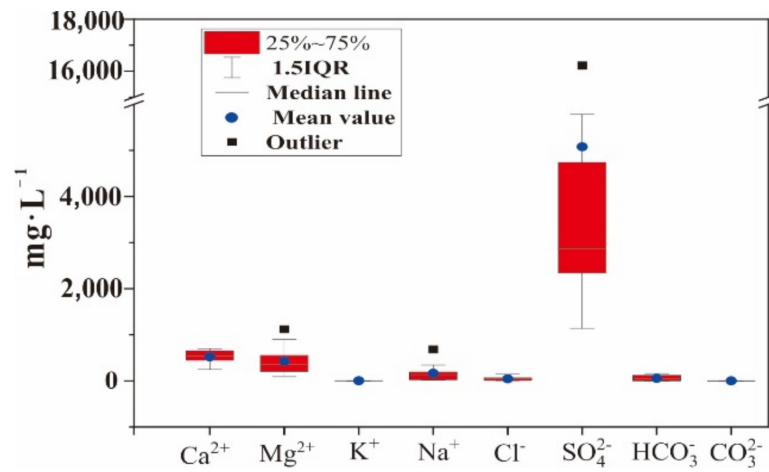


Figure 4. Box chart of ionic concentration in Acidic Mine Drainage (AMD).

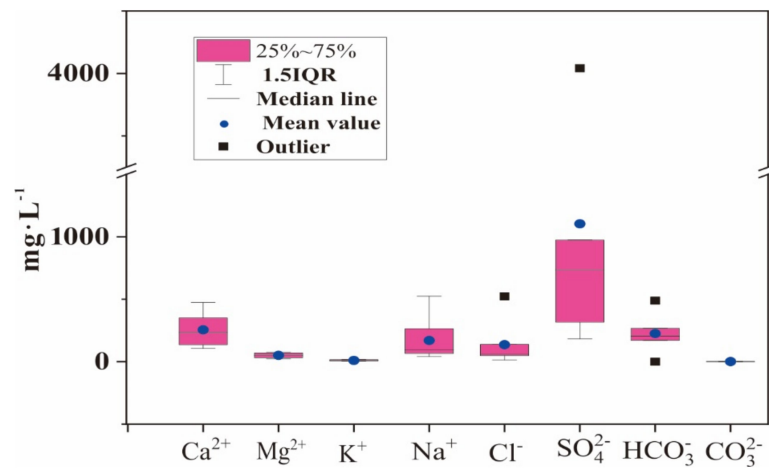


Figure 5. Box chart of ionic concentrations in the river.

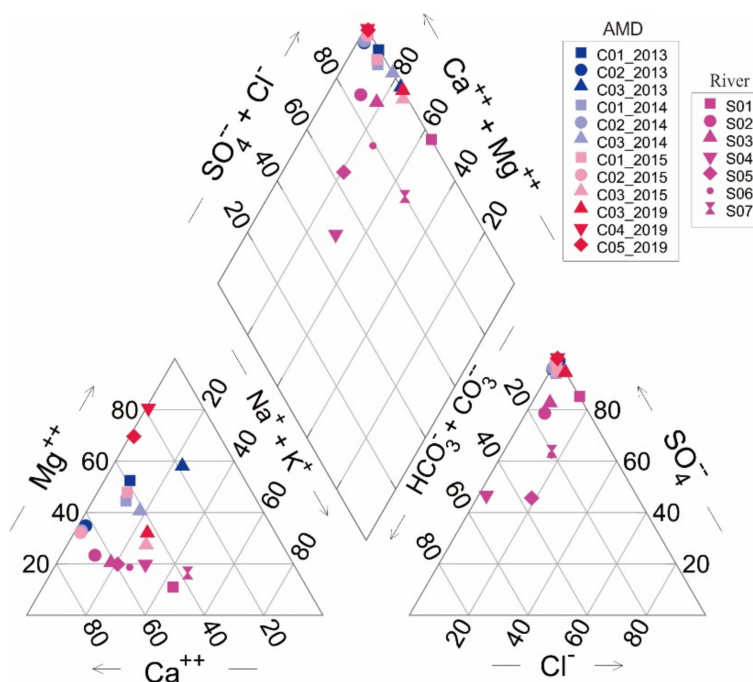


Figure 6. Piper diagram of ionic concentrations in the AMD or river.

3.2. Stable Isotopes

Table 1 and Figure 7 show a statistical summary of stable isotopes in the karst groundwater samples in the study area, the $\delta^{34}\text{S-SO}_4^{2-}$ values ranged from -6.11‰ to 27.68‰ , with an average of 13.93‰ . The δD values ranged from -74‰ to -49.8‰ , with an average of -68.62‰ . The $\delta^{18}\text{O}$ values were from -10.1‰ to -5.8‰ , with an average of -9.25‰ .

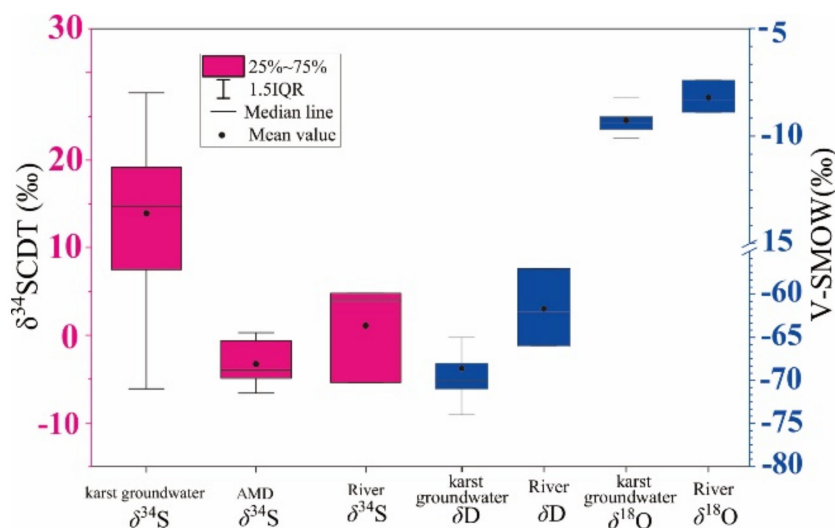


Figure 7. Box chart of stable isotopes in the AMD, river, or karst groundwater.

Table 2 and Figure 7 show the chemical properties and composition of AMD and river samples. The results showed that the $\delta^{34}\text{S-SO}_4^{2-}$ values for three surface water samples varied from -5.40‰ to 4.79‰ , with an average of 1.11‰ while seven samples from the acidic water at coal mines showed a range of $\delta^{34}\text{S-SO}_4^{2-}$ from -6.6‰ to 0.3‰ , with an average of -3.3‰ . The δD values ranged from -66‰ to -57‰ , with an average of -61.7‰ . Further, the $\delta^{18}\text{O}$ values were from -8.9‰ to -7.4‰ , with an average of -8.2‰ .

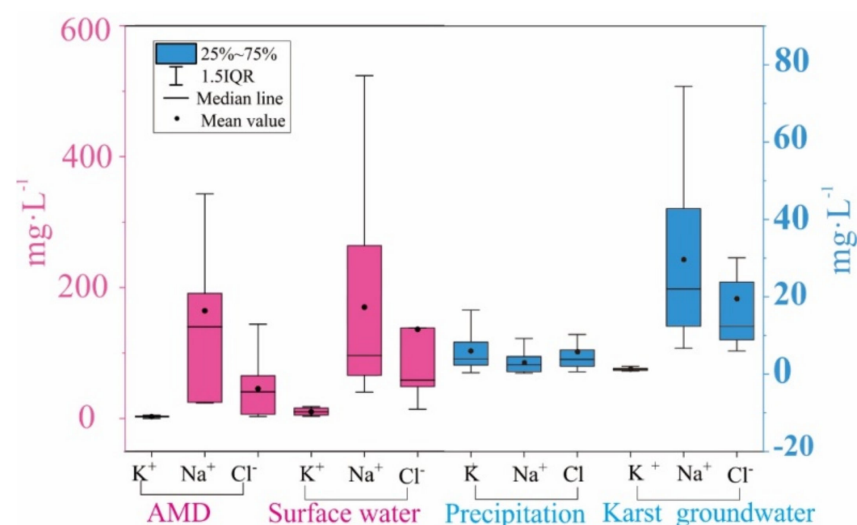
Table 2. The stable isotopes of AMD and River samples.

Sample NO.	Types	pH	T/°C	Date	$\text{mg}\cdot\text{L}^{-1}$			
					TDS	$\delta^{34}\text{S}$	δD	$\delta^{18}\text{O}$
C01_13	AMD	6.01	13	18 April 2013	4610	−3.3	/	/
C02_13	AMD	7.48	15.2	26 April 2013	3292	−6.6	/	/
C03_13	AMD	3.28	16.5	2 May 2013	8272	−4.9	/	/
C01_14	AMD	7.25	24	25 June 2014	4240	/	/	/
C02_14	AMD	7.27	22	23 June 2014	3518	/	/	/
C03_14	AMD	3.39	27.5	14 June 2014	5970	−4.6	/	/
C01_15	AMD	7.25	21	11 September 2015	3901	/	/	/
C02_15	AMD	7.17	20.8	17 September 2015	3310	/	/	/
C03_15	AMD	6.76	17.5	15 September 2015	1717	/	/	/
C04_19	AMD	2.83	19	30 April 2019	18936	−0.6	/	/
C05_19	AMD	2.75	16.5	30 April 2019	19094	0.3	/	/
S01	River	3.33	27	25 June 2014	6155	/	/	/
S02	River	7.25	18.2	14 June 2014	1702	−5.40	−66	−8.9
S03	River	7.27	23	16 June 2014	1496	/	/	/
S04	River	7.27	28.4	17 June 2014	748.3	/	/	/
S05	River	7.32	20	20 June 2014	522.5	/	/	/
S06	River	6.99	29	22 June 2014	1316	4.79	−57	−7.4
S07	River	7.03	26.3	22 June 2014	1679	3.94	−62	−8.3

4. Discussion

4.1. Sources of K^+ , Na^+ , and Cl^-

The main natural sources of K^+ , Na^+ , and Cl^- are atmospheric precipitation, human activity emissions, and dissolution of salt rocks. Figure 8 shows the concentrations of Na^+ , K^+ , and Cl^- in precipitation in the spring field were in ranges of 1.4 to 23.4 $\text{mg}\cdot\text{L}^{-1}$, 0.25 to 9.2 $\text{mg}\cdot\text{L}^{-1}$, and 1.6 to 24.7 $\text{mg}\cdot\text{L}^{-1}$, respectively. The concentrations of Na^+ , K^+ , and Cl^- in the surface water of the spring field showed ranges of 40.2 to 523.4 $\text{mg}\cdot\text{L}^{-1}$, 3.3 to 18.0 $\text{mg}\cdot\text{L}^{-1}$, and 3.1 to 144.0 $\text{mg}\cdot\text{L}^{-1}$, respectively. In contrast, the concentrations of Na^+ , K^+ , and Cl^- for the acidic water at coal mines were 23.7 to 343.0 $\text{mg}\cdot\text{L}^{-1}$, 0.1 to 3.8 $\text{mg}\cdot\text{L}^{-1}$, and 3.1 to 144.0 $\text{mg}\cdot\text{L}^{-1}$, respectively. This study also measured the concentrations of Na^+ , K^+ , and Cl^- for the karst groundwater, which showed ranges of 6.26 to 193.6 $\text{mg}\cdot\text{L}^{-1}$, 0.8 to 6.6 $\text{mg}\cdot\text{L}^{-1}$, and 6.0 to 164.9 $\text{mg}\cdot\text{L}^{-1}$, respectively. As shown in Figure 9, Cl^- has a positive correlation with Na^+ and K^+ in karst groundwater. Na^+ , K^+ , and Cl^- mainly originated from urban domestic sewage or coal mine drainage [59–61].

**Figure 8.** Box chart of K^+ , Na^+ , and Cl^- .

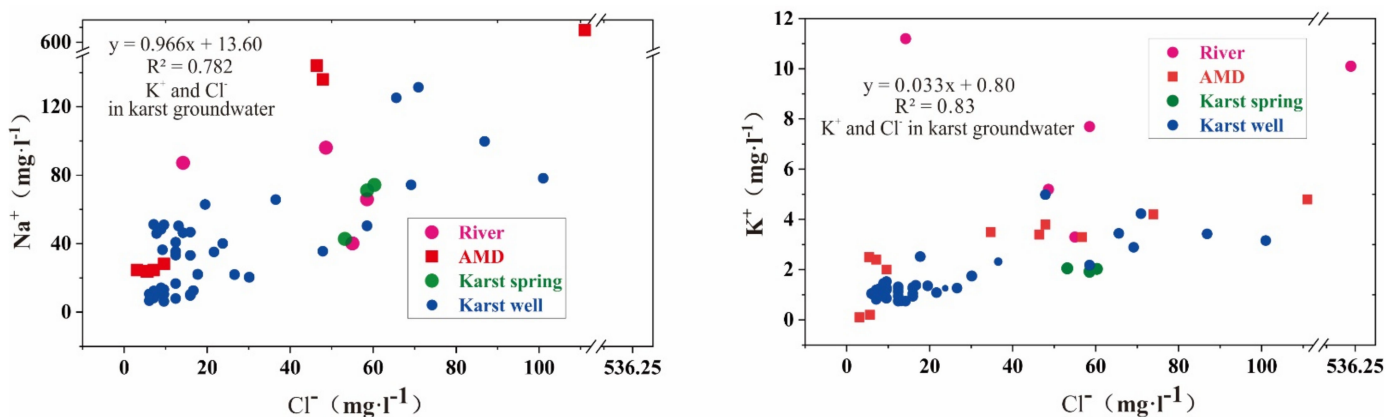


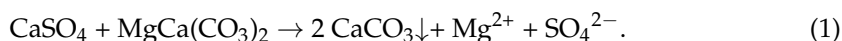
Figure 9. Relationships between (a) K^+ vs. Cl^- in karst groundwater (b) Na^+ vs. Cl^- in karst groundwater.

4.2. Sources of Ca^{2+} , Mg^{2+} and HCO_3^-

This study showed that the karst groundwater has the main ions of Ca^{2+} , Mg^{2+} , and HCO_3^- , which are mainly derived from dissolution of carbonate rocks and gypsum as well as dedolomitization. There are large differences in the mechanisms of groundwater runoff.

4.2.1. Dissolution of Carbonate Rocks and Gypsum

The dissolution of calcite and dolomite in Ordovician strata is the main source of Ca^{2+} , Mg^{2+} , and HCO_3^- . The dissolution equations are shown in Equation (1):



The dissolution of gypsum may cause an increase of Ca^{2+} and SO_4^{2-} in the karst groundwater. Figure 10a shows a strong positive correlation between Ca^{2+} and Mg^{2+} in the karst groundwater. Figure 10b also shows a strong positive correlation between Ca^{2+} and SO_4^{2-} in the karst groundwater, indicating that the dissolution of gypsum plays an important role in the concentration of Ca^{2+} and SO_4^{2-} .

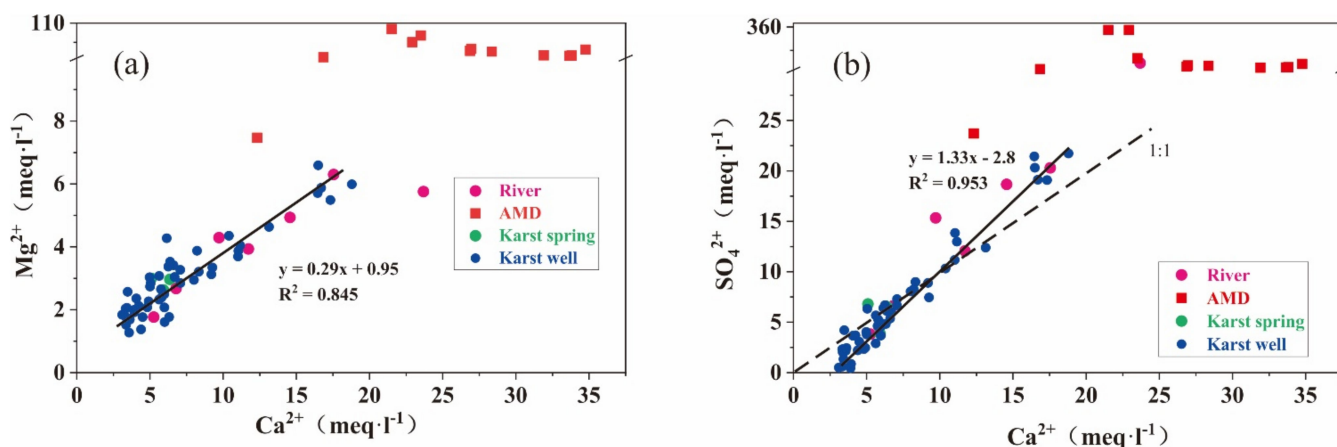


Figure 10. (a) Relationships between Mg^{2+} vs. Ca^{2+} (b) Relationships between SO_4^{2-} vs. Ca^{2+} .

4.2.2. Dedolomitization

As the solubility of $CaSO_4$ is greater than that of $CaCO_3$ and $CaMg(CO_3)_2$ due to the coion effect, the precipitation of calcium carbonate ($CaCO_3$) will occur in order to maintain the equilibrium of Ca^{2+} concentration. When the precipitation of $CaCO_3$ takes away part of the HCO_3^- from the solution, dolomite will be dissolved to maintain the mass balance of HCO_3^- concentration, which is called dedolomitization [62,63].

We assumed that the dedolomitization is real. Dedolomitization as described in Equation (1) leads to an increase of concentration in SO_4^{2-} and Mg^{2+} in the karst groundwater and precipitation of calcite; subsequently, the mass concentrations of HCO_3^- and Ca^{2+} remain unchanged. Figure 11 shows that SO_4^{2-} and Mg^{2+} have a strong correlation ($R^2 = 0.87$), demonstrating that dedolomitization is the main source of Mg^{2+} .

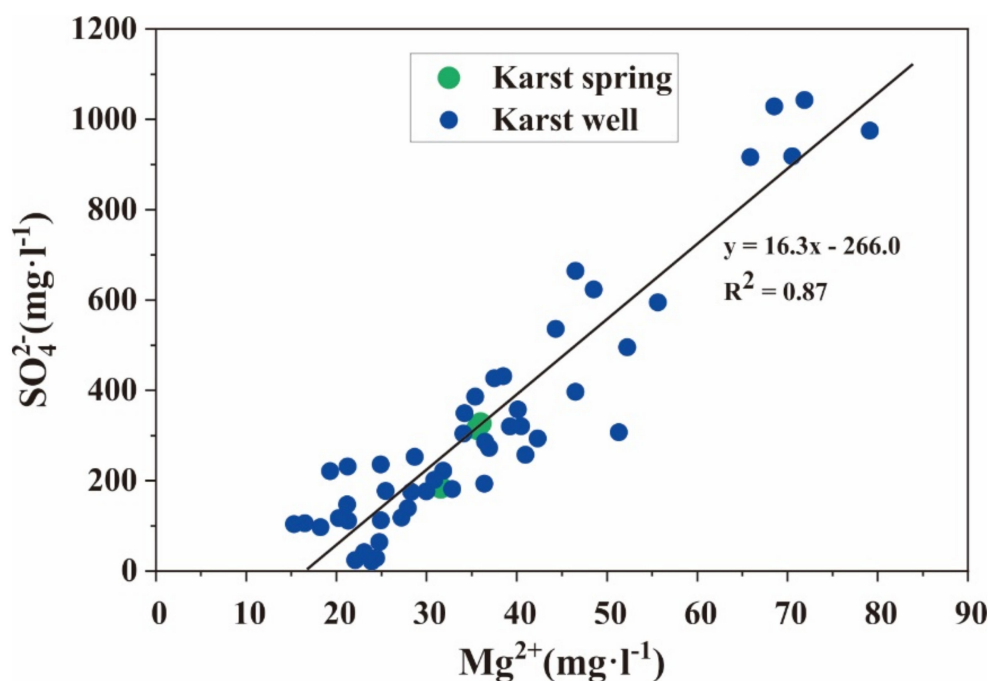


Figure 11. Relationships between SO_4^{2-} vs. Mg^{2+} .

4.3. Water-Rock Interaction

The chemical composition of the karst groundwater in the Niangziguan spring field is mainly dependent on the dissolution of calcite, dolomite, and gypsum. Figure 12a shows the relationship between $\text{SO}_4^{2+} + \text{Cl}^-$ and HCO_3^- . The points below the 1:1 line represent that the dissolution of evaporite is accompanied. The results imply that the karst groundwater in the Niangziguan spring field is mainly affected by the dissolution of carbonate rocks, along with the dissolution of evaporites (e.g., gypsum, Cl^- in AMD or rivers, etc.). Figure 12b also shows the relationship between $\text{SO}_4^{2+} + \text{HCO}_3^-$ and $\text{Ca}^{2+} + \text{Mg}^{2+}$. Most analytical points are lying on the straight line or below the 1:1 line, indicating that karst groundwater is affected by acid drainage and surface water. The relationship between $\text{Na}^+ + \text{K}^+ - \text{Cl}^-$ and $\text{Ca}^{2+} + \text{Mg}^{2+} - \text{SO}_4^{2+} - \text{CO}_3^-$ is shown in Figure 12c. Most of the analytical points from the runoff area lie near the cation exchange line, which means that the hydrochemistry of groundwater is dependent on not only the dissolution of calcite, dolomite, and gypsum but also on cation exchange. Figure 12d shows the relationship between $\text{Ca}^{2+} / \text{Na}^+$ and $\text{HCO}_3^- / \text{Na}^+$ to evaluate the effects of materials from different sources (evaporite, silicate, precipitation, and carbonate rocks) in the processes of the groundwater circulation. The result demonstrates that the main factors influencing the hydrochemical features of the karst groundwater in the Niangziguan spring field are precipitation and dissolution of carbonate rocks.

The TDS values, a comprehensive indicator of water quality, obtained from 52 water samples in the karst groundwater within the study area ranged from 280.3 to 1859 $\text{mg}\cdot\text{L}^{-1}$, an average of 775.7 $\text{mg}\cdot\text{L}^{-1}$. The TDS values in the karst groundwater are larger in order of the recharge area, runoff area, discharge area, and the detention area. Figure 13 show the relationship between TDS and SO_4^{2-} . It is prominent that TDS has a strong linear correlation with SO_4^{2-} contents ($R^2 = 0.922$). SO_4^{2-} in regional karst groundwater is mainly derived from the dissolution of gypsum in the Ordovician carbonate rocks while SO_4^{2-} in

acidic water is from coal mines and meteoric precipitation. The average TDS values in the Niangziguan spring field is 688.6 mg·L⁻¹, lower than the average values analyzed in this study, because the TDS values in the karst water are affected by the runoff condition, the dissolution of gypsum, and the pollution caused by acidic water from coal mines.

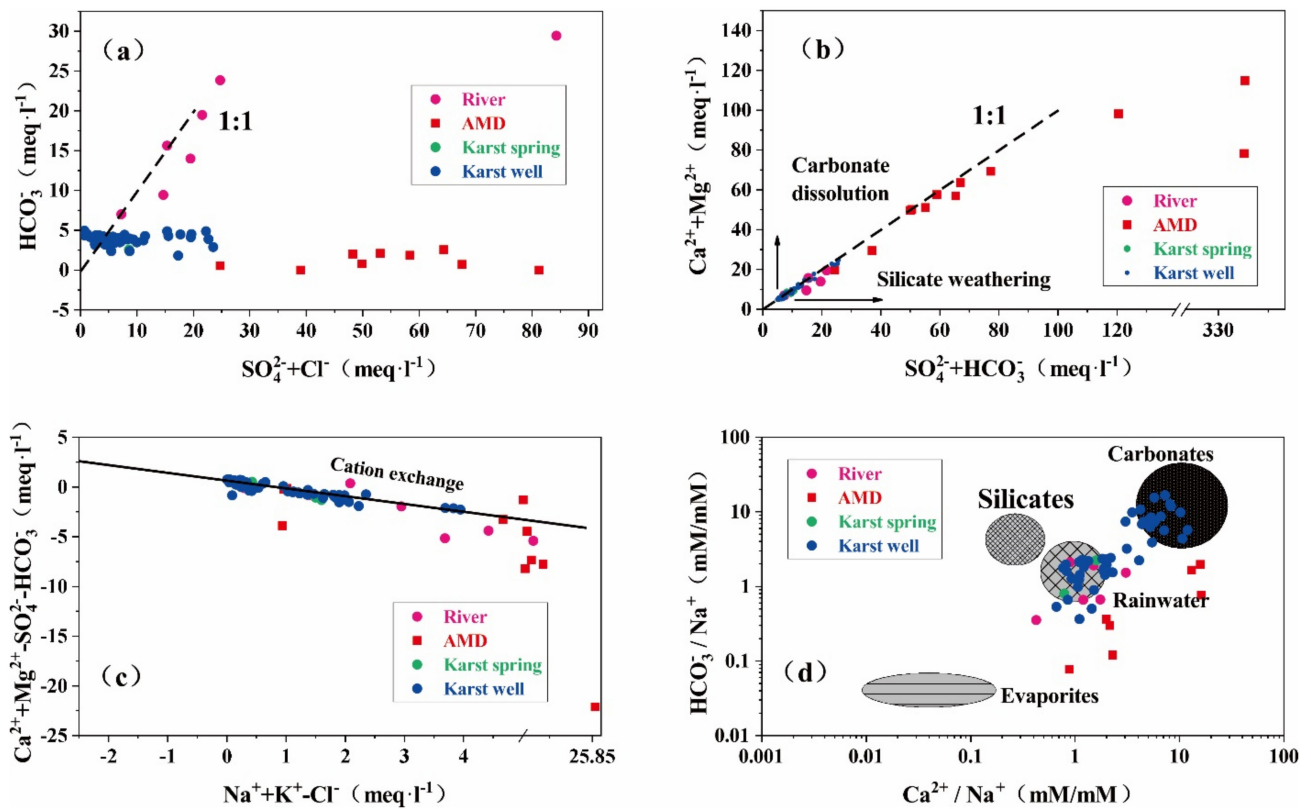


Figure 12. Ion relationship involving karst groundwater in the Niangziguan Spring Catchment (a) Relationships between Mg²⁺ vs. SO₄²⁻, (b) SO₄²⁻+HCO₃⁻ vs. Ca²⁺+Mg²⁺, (c) Na⁺+K⁺-Cl⁻ vs. Ca²⁺+Mg²⁺-SO₄²⁺-CO₃⁻, (d) Ca²⁺/Na⁺ vs. HCO₃⁻/Na⁺.

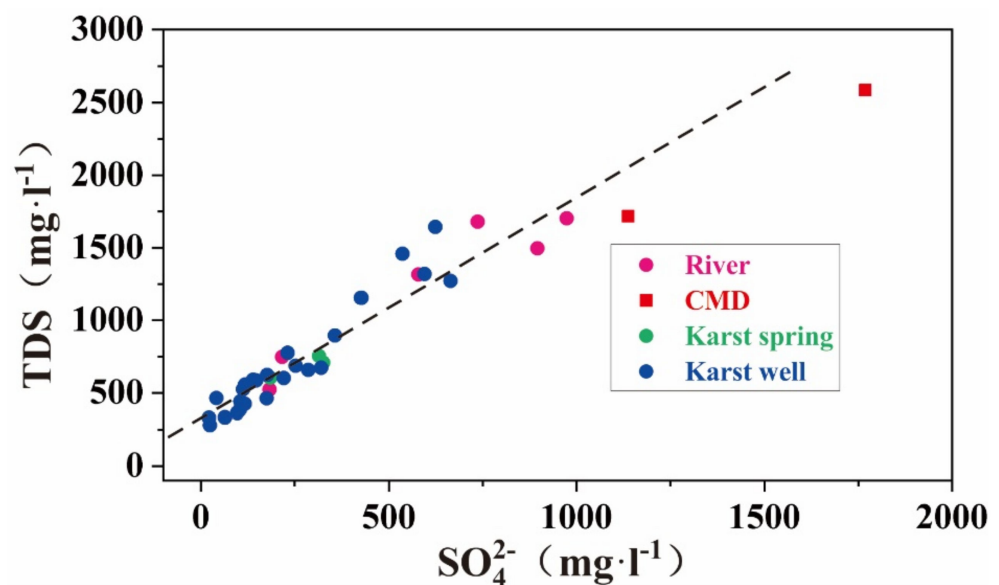


Figure 13. Relationships between TDS vs. SO₄²⁻.

4.4. Supply Source of Karst Groundwater

The $\delta^{34}\text{S}\text{-SO}_4^{2-}$ isotope has been widely used to trace the source of sulfate in water. In addition, H-O isotopes are ideal tracers to detect the origin and evolution of groundwater. Thus, these stable isotopes in groundwater were used to identify the recharge sources of groundwater in the study area.

4.4.1. Recharge Sources

The δD values for the karst groundwater samples in the study area ranged from -74‰ to -49.8‰ , an average of -68.62‰ while the $\delta^{18}\text{O}$ values ranged from -10.1‰ to -5.8‰ , an average of -9.25‰ . Figure 14 shows the relationship between δD and $\delta^{18}\text{O}$. The result shows that the intercept and slope of the $\delta\text{D}\text{-}\delta^{18}\text{O}$ relation line are both lower than the global precipitation line ($\delta\text{D} = 8\delta^{18}\text{O} + 10$) due to an inland arid climate in the study area. The results also show that meteoric precipitation is the main recharge source of karst water in the Niangziguan spring field. The H-O isotopic composition of surface water was similar to that of the karst groundwater in the runoff area, implying that the karst groundwater is mostly recharged from the seepage of surface water.

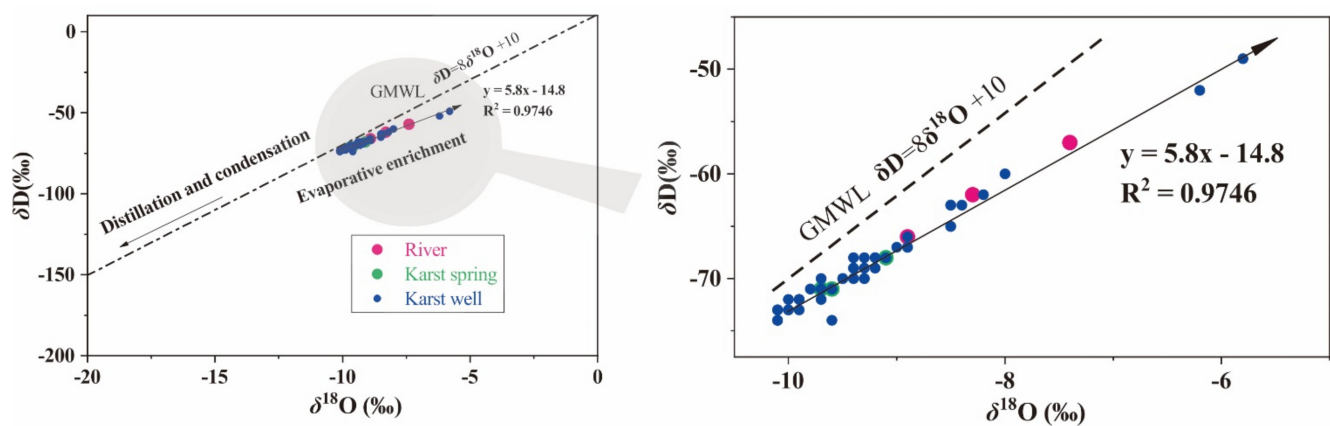


Figure 14. Relationships between δD vs. $\delta^{18}\text{O}$ for the karst groundwater.

4.4.2. Sources of SO_4^{2-}

While the surface water showed SO_4^{2-} concentrations ranging from 183.2 to 4042 $\text{mg}\cdot\text{L}^{-1}$, an average of 1089.6 $\text{mg}\cdot\text{L}^{-1}$, SO_4^{2-} concentrations for the acidic water in coal mines ranged from 1138 to 16218 $\text{mg}\cdot\text{L}^{-1}$, an average of 5079 $\text{mg}\cdot\text{L}^{-1}$. In contrast, the karst groundwater showed SO_4^{2-} concentrations ranging from 21.7 to 1043 $\text{mg}\cdot\text{L}^{-1}$, an average of 323.9 $\text{mg}\cdot\text{L}^{-1}$ (Figure 15). Precipitation and dissolution of gypsum, oxidation of FeS_2 in coal-bearing strata are the sources of SO_4^{2-} in the karst groundwater. However, SO_4^{2-} in precipitation (23.95 $\text{mg}\cdot\text{L}^{-1}$ on average) has little influence on the karst groundwater. Therefore, it was assumed that most SO_4^{2-} is sourced from both oxidation of FeS_2 and dissolution of gypsum. The $\delta^{34}\text{S}$ values of SO_4^{2-} formed dissolution of gypsum and formed oxidation of FeS_2 are 26.2‰ (the mean value of gypsum samples) and -3.3‰ (the mean value of AMD in Niangziguan spring catchment), respectively (Figure 16). A ^{34}S isotopic analysis was conducted to determine the source of SO_4^{2-} by calculating the proportion of SO_4^{2-} sourced from FeS_2 oxidation in the karst groundwater by mass balance. As shown in Table 3, the proportions for the main discharge points (N50, N51, and N52) were 60.6%, 30.3%, and 26.0%, respectively.

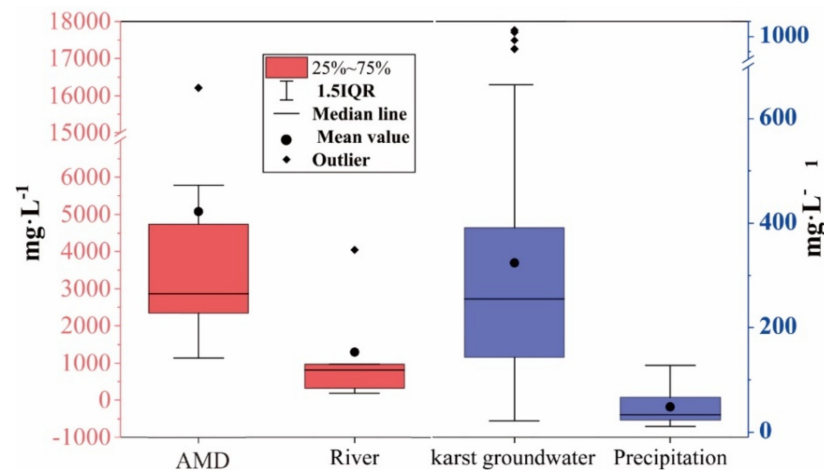


Figure 15. Box chart of SO_4^{2-} .

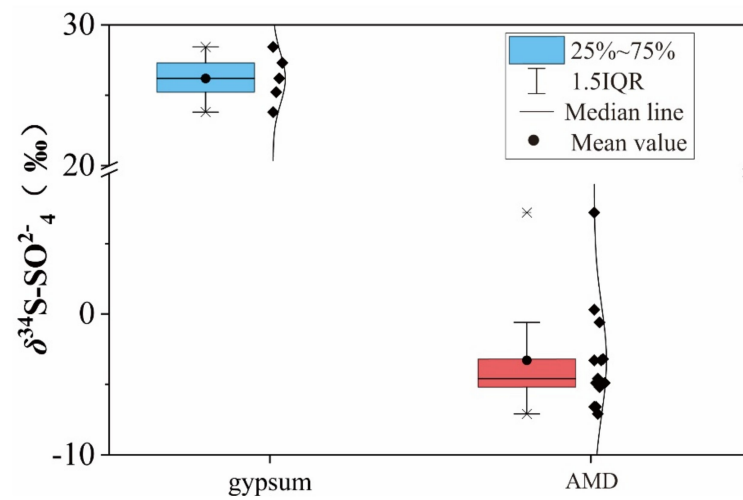


Figure 16. Box chart of $\delta^{34}\text{S}$ values of SO_4^{2-} forming the dissolution of gypsum and forming the oxidation of FeS_2 .

Table 3. Ratio of sulfate ion from pyrite oxidation in the calculation of water/%.

Sample NO.	$\delta^{34}\text{S}$ (‰)	From FeS_2 (%)	Sample NO.	$\delta^{34}\text{S}$ (‰)	From FeS_2 (%)	Sample NO.	$\delta^{34}\text{S}$ (‰)	From FeS_2 (%)
N01	-6.11	100	N19	11.86	54.7	N37	20.52	19.3
N02	-3.54	100	N20	12.24	53.4	N38	21.15	17.1
N03	-0.21	89.5	N21	12.31	53.2	N39	21.18	17.0
N04	0.77	86.2	N22	13.55	49.0	N40	22.06	14.0
N05	4.03	75.2	N23	14.1	47.1	N41	22.6	12.2
N06	4.24	74.4	N24	14.6	45.4	N42	22.65	12.0
N07	4.84	72.4	N25	14.66	45.2	N43	24.47	5.9
N08	4.97	72.0	N26	15.12	43.7	N44	24.52	5.7
N09	5.98	68.5	N27	16.45	39.2	N45	24.62	5.4
N10	6.14	68.0	N28	16.87	37.7	N46	24.87	4.5
N11	6.37	67.2	N29	17	37.3	N47	24.97	4.2
N12	7.22	64.3	N30	17.02	37.2	N48	26.06	0.5
N13	7.43	63.6	N31	17.3	36.3	N49	27.68	0.0
N14	7.49	63.4	N32	17.46	35.7	N50	8.31	60.6
N15	8.56	59.8	N33	17.98	34.0	N51	17.26	30.3
N16	9.41	56.9	N34	18.03	33.8	N52	18.54	26.0
N17	10.31	53.9	N35	19.08	30.2			
N18	10.43	53.5	N36	19.16	30.0			

5. Conclusions

The karst groundwater in the Niangziguan spring field was mainly classified into $\text{SO}_4\cdot\text{HCO}_3\text{-Ca}\cdot\text{Mg}$, $\text{HCO}_3\text{-SO}_4\text{-Ca}\cdot\text{Mg}$, and $\text{SO}_4\text{-Ca}$ types. The SO_4^{2-} exceeding ratio of karst groundwater samples in this study was 51.9%.

K^+ , Cl^- , and Na^+ are mainly sourced from urban sewage and coal mine drainage. Dedolomitization gradually led to an increase of Mg^{2+} , especially in the processes of the groundwater runoff. While the main sources of SO_4^{2-} supply were the dissolution of gypsum and the oxidation of FeS_2 in coal-bearing strata, the hydrochemical characteristics of the study area were mainly affected by dedolomitization, the dissolution of dolomite, salt, rock and gypsum.

The isotopic analyses found that acidic water in coal mines contributed to the pollution of the karst groundwater at different degrees. In the groundwater of the Niangziguan spring field, the proportions of SO_4^{2-} derived from FeS_2 oxidation were 60.6% (N50), 30.3% (N51), and 26.0% (N52), respectively.

The acid water of coal mine directly recharges and pollutes karst groundwater through faults or abandoned boreholes, or discharges to rivers and indirectly pollutes karst groundwater through river infiltration in carbonate exposed areas. The main cause for the rapid growth of sulfate in karst groundwater is acid water from abandoned coal mines.

Author Contributions: Data curation, C.T.; Formal analysis, C.T.; Funding acquisition, Y.L.; Investigation, C.T. and Y.L.; Methodology, C.T.; Project administration, Y.L.; Software, C.T.; Supervision, H.J.; Writing—original draft, C.T.; Writing—review & editing, C.T. and H.J. All authors have read and agreed to the published version of the manuscript.

Funding: This research were funded by The National Natural Science Foundation of China, grant number 41672253, The China Geological Survey Project of the Ministry of Natural Resources, and grant number DD20190334 and Basic scientific research project of Chinese academy of geological sciences and grant number 2020010.

Institutional Review Board Statement: “Not applicable” for studies not involving humans or animals.

Informed Consent Statement: “Not applicable” for studies not involving humans.

Data Availability Statement: All data, models, and code generated or used during the study appear in the submitted article.

Conflicts of Interest: The authors declare no conflict of interest.

References

1. Ford, D.C.; Williams, P. *Karst Hydrogeology and Geomorphology*; Wiley: Hoboken, NJ, USA, 2007; ISBN 9780470849965.
2. Nerantzaki, S.D.; Nikolaidis, N.P. The response of three Mediterranean karst springs to drought and the impact of climate change. *J. Hydrol.* **2020**, 125296. [[CrossRef](#)]
3. Hasan, O.; Miko, S.; Ilijani, N.; Brunović, D.; Dedić, Ž.; Miko, M.Š.; Peh, Z. Discrimination of topsoil environments in a karst landscape: An outcome of a geochemical mapping campaign. *Geochem. Trans.* **2020**, 21, 1. [[CrossRef](#)] [[PubMed](#)]
4. Frank, S.; Goepfert, N.; Goldscheider, N. Fluorescence-based multi-parameter approach to characterize dynamics of organic carbon, faecal bacteria and particles at alpine karst springs. *Sci. Total Environ.* **2018**, 1446–1459. [[CrossRef](#)] [[PubMed](#)]
5. Liang, Y.; Gao, X.; Zhao, C.; Tang, C.; Shen, H.; Wang, Z.; Wang, Y. Review: Characterization, evolution, and environmental issues of karst water systems in Northern China. *Hydrogeol. J.* **2018**, 26, 1371–1385. [[CrossRef](#)]
6. Yang, P.; Li, Y.; Groves, C.; Hong, A. Coupled hydrogeochemical evaluation of a vulnerable karst aquifer impacted by septic effluent in a protected natural area. *Sci. Total Environ.* **2019**, 658, 1475–1484. [[CrossRef](#)]
7. Ren, K.; Pan, X.; Zeng, J.; Yuan, D. Contaminant sources and processes affecting spring water quality in a typical karst basin (Hongjiadu Basin, SW China): Insights provided by hydrochemical and isotopic data. *Environ. Sci. Pollut. Res.* **2019**, 26, 31354–31367. [[CrossRef](#)]
8. Wu, Y.; Luo, Z.; Luo, W.; Ma, T.; Wang, Y. Multiple isotope geochemistry and hydrochemical monitoring of karst water in a rapidly urbanized region. *J. Contam. Hydrol.* **2018**, 218, 44–58. [[CrossRef](#)]
9. Cao, X.; Zhou, S.; Xie, F.; Rong, R.; Wu, P. The distribution of rare earth elements and sources in Maoshitou reservoir affected by acid mine drainage, Southwest China. *J. Geochem. Explor.* **2019**, 202, 92–99. [[CrossRef](#)]

10. Ren, K.; Zeng, J.; Liang, J.; Yuan, D.; Jiao, Y.; Peng, C.; Pan, X. Impacts of acid mine drainage on karst aquifers: Evidence from hydrogeochemistry, stable sulfur and oxygen isotopes. *Sci. Total Environ.* **2020**, *10*, 143223. [[CrossRef](#)]
11. Vesper, D.J.; White, W.B. Metal transport to karst springs during storm flow: An example from Fort Campbell, Kentucky/Tennessee, USA. *J. Hydrol.* **2003**, *276*, 20–36. [[CrossRef](#)]
12. Zhang, X.; Guo, J.; Hu, Q.; Gao, X.; Li, C.; Luo, M.; Wang, Y. Effects of Fe-rich acid mine drainage on percolation features and pore structure in carbonate rocks. *J. Hydrol.* **2020**, *591*, 125571. [[CrossRef](#)]
13. Boumaiza, L.; Chesnaux, R.; Drias, T.; Walter, J.; Huneau, F.; Garel, E.; Knoeller, K.; Stumpp, C. Identifying groundwater degradation sources in a Mediterranean coastal area experiencing significant multi-origin stresses. *Sci. Total Environ.* **2020**, *746*, 141203. [[CrossRef](#)] [[PubMed](#)]
14. Kaown, D.; Koh, D.C.; Mayer, B.; Lee, K.-K. Identification of nitrate and sulfate sources in groundwater using dual stable isotope approaches for an agricultural area with different land use (Chuncheon, mid-eastern Korea). *Agric. Ecosyst. Environ.* **2009**, *132*, 223–231. [[CrossRef](#)]
15. Lang, Y.C.; Liu, C.Q.; Li, S.L.; Zhao, Z.Q.; Zhou, Z.-H. Tracing natural and anthropogenic sources of dissolved sulfate in a karst region by using major ion chemistry and stable sulfur isotopes. *Appl. Geochem.* **2011**, *26*, S202–S205. [[CrossRef](#)]
16. Obeidat, M.; Awawdeh, M.; Matiatos, I.; Al-Ajlouni, A.; Al-Mughaid, H. Identification and apportionment of nitrate sources in the phreatic aquifers in Northern Jordan using a dual isotope method ($\delta^{15}\text{N}$ and $\delta^{18}\text{O}$ of NO_3^-). *Groundw. Sustain. Dev.* **2020**. [[CrossRef](#)]
17. Yakovlev, V.; Vystavna, Y.; Diadin, D.; Vergeles, Y. Nitrates in springs and rivers of East Ukraine: Distribution, contamination and fluxes. *Appl. Geochem.* **2015**, *53*, 71–78. [[CrossRef](#)]
18. Jakóbczyk-Karpierz, S.; Sitek, S.; Jakobsen, R.; Kowalczyk, A. Geochemical and isotopic study to determine sources and processes affecting nitrate and sulphate in groundwater influenced by intensive human activity—Carbonate aquifer Gliwice (southern Poland). *Appl. Geochem.* **2017**, *76*, 168–181. [[CrossRef](#)]
19. Cao, X.; Wu, P.; Zhou, S.; Sun, J.; Han, Z. Tracing the origin and geochemical processes of dissolved sulphate in a karst-dominated wetland catchment using stable isotope indicators. *J. Hydrol.* **2018**, *562*, 210–222. [[CrossRef](#)]
20. Zhu, H.; Wu, L.; Xin, C.; Yu, S.; Guo, Y.; Wang, J. Impact of anthropogenic sulfate deposition via precipitation on carbonate weathering in a typical industrial city in a karst basin of southwest China: A case study in Liuzhou. *Appl. Geochem.* **2019**, *110*, 104417. [[CrossRef](#)]
21. Martin, J.B.; Kurz, M.J.; Khadka, M.B. Climate control of decadal-scale increases in apparent ages of eogenetic karst spring water. *J. Hydrol.* **2016**, *540*, 988–1001. [[CrossRef](#)]
22. Stange, C.; Tiehm, A. Occurrence of antibiotic resistance genes and microbial source tracking markers in the water of a karst spring in Germany. *Sci. Total Environ.* **2020**, *742*, 140529. [[CrossRef](#)] [[PubMed](#)]
23. Jeelani, G.; Shah, R.A.; Deshpande, R.D.; Fryar, A.E.; Perrin, J.; Mukherjee, A. Distinguishing and estimating recharge to karst springs in snow and glacier dominated mountainous basins of the western Himalaya, India. *J. Hydrol.* **2017**, *550*, 239–252. [[CrossRef](#)]
24. Karmann, I.; Cruz, F.W.; Viana, O.; Burns, S.J. Climate influence on geochemistry parameters of waters from Santana-Pérolas cave system, Brazil. *Chem. Geol.* **2007**, *244*, 232–247. [[CrossRef](#)]
25. Qin, R.; Wu, Y.; Xu, Z.; Xie, D.; Zhang, C. Assessing the impact of natural and anthropogenic activities on groundwater quality in coastal alluvial aquifers of the lower Liaohe River Plain, NE China. *Appl. Geochem.* **2013**, *31*, 142–158. [[CrossRef](#)]
26. Capaccioni, B.; Vaselli, O.; Tassi, F.; Santo, A.P.; Huertas, A.D. Hydrogeochemistry of the thermal waters from the Sciacca Geothermal Field (Sicily, southern Italy). *J. Hydrol.* **2011**, *396*, 292–301. [[CrossRef](#)]
27. Kohfahl, C.; Sprenger, C.; Herrera, J.B.; Meyer, H.; Chacón, F.F.; Pekdeger, A. Recharge sources and hydrogeochemical evolution of groundwater in semiarid and karstic environments: A field study in the Granada Basin (Southern Spain). *Appl. Geochem.* **2008**, *23*, 846–862. [[CrossRef](#)]
28. Pasvanoğlu, S. Hydrogeochemistry of thermal and mineralized waters in the Diyadin (Ağrı) area, Eastern Turkey. *Appl. Geochem.* **2013**, *38*, 70–81. [[CrossRef](#)]
29. Shi, M.; Wang, S.; Argiriou, A.A.; Zhang, M.; Guo, R.; Jiao, R.; Kong, J.; Zhang, Y.; Qiu, X.; Zhou, S. Stable Isotope Composition in Surface Water in the Upper Yellow River in Northwest China. *Water* **2019**, *11*, 967. [[CrossRef](#)]
30. Ekholm, P.; Lehtoranta, J.; Taka, M.; Sallantausta, T.; Riihimäki, J. Diffuse sources dominate the sulfate load into Finnish surface waters. *Sci. Total Environ.* **2020**, *748*, 141297. [[CrossRef](#)]
31. Saldanha, M.M.; Araújo, I.C.S.; Triguineli, M.V.; Vaz, D.P.; Ferreira, F.N.A.; Albergaria, J.D.S.; Fontes, D.O.; Lara, L.J.C. Relative bioavailability of manganese in relation to proteinate and sulfate sources for broiler chickens from one to 20 d of age. *Poult. Sci.* **2020**, *99*, 5647–5652. [[CrossRef](#)]
32. Torres-Martínez, J.A.; Mora, A.; Knappett, P.S.K.; Ornelas-Soto, N.; Mahlkecht, J. Tracking nitrate and sulfate sources in groundwater of an urbanized valley using a multi-tracer approach combined with a Bayesian isotope mixing model. *Water Res.* **2020**, *182*, 115962. [[CrossRef](#)] [[PubMed](#)]
33. Zak, D.; Hupfer, M.; Cabezas, A.; Jurasinski, G.; Audet, J.; Kleeberg, A.; McInnes, R.; Kristiansen, S.M.; Petersen, R.J.; Liu, H.; et al. Sulphate in freshwater ecosystems: A review of sources, biogeochemical cycles, ecotoxicological effects and bioremediation. *Earth-Sci. Rev.* **2020**. [[CrossRef](#)]

34. Zhang, Q.; Wang, H.; Lu, C. Tracing sulfate origin and transformation in an area with multiple sources of pollution in northern China by using environmental isotopes and Bayesian isotope mixing model. *Environ. Pollut.* **2020**, *265*, 115105. [[CrossRef](#)] [[PubMed](#)]
35. Zheng, L.; Chen, X.; Dong, X.; Wei, X.; Jiang, C.; Tang, Q. Using $\delta^{34}\text{S}\text{-SO}_4$ and $\delta^{18}\text{O}\text{-SO}_4$ to trace the sources of sulfate in different types of surface water from the Linhuan coal-mining subsidence area of Huaibei, China. *Ecotoxicol. Environ. Saf.* **2019**, *181*, 231–240. [[CrossRef](#)]
36. Chen, X.; Sun, Y.; Huang, R. Role of hydro-geochemical functions on karst critical zone hydrology for sustainability of water resources and ecology in Southwest China. *Acta Geochim.* **2017**, *36*, 494–497. [[CrossRef](#)]
37. He, S.; Zhu, L.; Yang, R.; Shen, Z.; Yu, X. The geochemical characteristics of aqueous rare-earth elements in shallow karst groundwater in Guiyang City, China. *Chin. J. Geochem.* **2011**, *30*, 114–124. [[CrossRef](#)]
38. Holland, M.; Witthüser, K.T. Geochemical characterization of karst groundwater in the cradle of humankind world heritage site. *S. Afr. Environ. Geol.* **2008**, *57*, 513–524. [[CrossRef](#)]
39. Jing, M.; Chen, W.; Zheng, T.; Liao, Y.; Ellis Burnet, J.; Xu, M.; Yang, C.; Shen, L.; Liang, M. Water geochemical characteristic variations in and around a karst-dominated natural reserve area, southwestern China. *Environ. Earth Sci.* **2011**, *64*, 1051–1058. [[CrossRef](#)]
40. Rosales Lagarde, L.; Boston, P.J.; Campbell, A.R.; Hose, L.D.; Axen, G.; Stafford, K.W. Hydrogeology of northern Sierra de Chiapas, Mexico: A conceptual model based on a geochemical characterization of sulfide-rich karst brackish springs. *Hydrogeol. J.* **2014**, *22*, 1447–1467. [[CrossRef](#)]
41. Tuyukina, T.Y. Geochemical studies of northern taiga (gypsum) karst ecosystems and their high vulnerability to natural and anthropogenic hazards. *Environ. Geol.* **2008**, *58*, 269–274. [[CrossRef](#)]
42. Yang, M.; Lu, Y.; Zhang, F.E.; Zhang, S.; Yin, M.; Wu, G. Identification of geochemical processes by hydrogeochemical analysis in karst aquifers of a semi-arid region, Northern China. *Carbonates Evaporites* **2017**, *34*, 297–313. [[CrossRef](#)]
43. Brkić, Ž.; Kuhta, M.; Hunjak, T. Groundwater flow mechanism in the well-developed karst aquifer system in the western Croatia: Insights from spring discharge and water isotopes. *Catena* **2018**, *161*, 14–26. [[CrossRef](#)]
44. Alves, M.; Galvão, P.; Aranha, P. Karst Hydrogeological Controls and Anthropogenic Effects in an Urban Lake. *J. Hydrol.* **2020**. [[CrossRef](#)]
45. Ayadi, Y.; Mokadem, N.; Besser, H.; Khelifi, F.; Harabi, S.; Hamad, A.; Boyce, A.; Laouar, R.; Hamed, Y. Hydrochemistry and stable isotopes ($\delta^{18}\text{O}$ and $\delta^2\text{H}$) tools applied to the study of karst aquifers in southern mediterranean basin (Teboursouk area, NW Tunisia). *J. Afr. Earth Sci.* **2018**, *137*, 208–217. [[CrossRef](#)]
46. Gil-Márquez, J.M.; Andreo, B.; Mudarra, M. Combining hydrodynamics, hydrochemistry, and environmental isotopes to understand the hydrogeological functioning of evaporite-karst springs. An example from southern Spain. *J. Hydrol.* **2019**, *576*, 299–314. [[CrossRef](#)]
47. Herms, I.; Jódar, J.; Soler, A.; Vadillo, I.; Lambán, L.J.; Martos-Rosillo, S.; Núñez, J.A.; Arnó, G.; Jorge, J. Contribution of isotopic research techniques to characterize high-mountain-Mediterranean karst aquifers: The Port del Comte (Eastern Pyrenees) aquifer. *Sci. Total Environ.* **2019**, *656*, 209–230. [[CrossRef](#)]
48. Husic, A.; Fox, J.; Adams, E.; Pollock, E.; Ford, W.; Agouridis, C.; Backus, J. Quantification of nitrate fate in a karst conduit using stable isotopes and numerical modeling. *Water Res.* **2020**, *170*, 115348. [[CrossRef](#)]
49. Ji, H.; Chang, C.; Beckford, H.O.; Song, C.; Blake, R.E. New perspectives on lateritic weathering process over karst area—Geochemistry and Si-Li isotopic evidence. *Catena* **2020**. [[CrossRef](#)]
50. Ma, R.; Wang, Y.; Sun, Z.; Zheng, C.; Ma, T.; Prommer, H. Geochemical evolution of groundwater in carbonate aquifers in Taiyuan, northern China. *Appl. Geochem.* **2011**, *26*, 884–897. [[CrossRef](#)]
51. Hong Quang, N.; Tuan, V.A.; Thi Thu Hang, L.; Manh Hung, N.; Thi The, D.; Thi Dieu, D.; Duc Anh, N.; Hackney, C.R. Hydrological/Hydraulic Modeling-Based Thresholding of Multi SAR Remote Sensing Data for Flood Monitoring in Regions of the Vietnamese Lower Mekong River Basin. *Water* **2019**, *12*, 71. [[CrossRef](#)]
52. Sağır, Ç.; Kurtuluş, B.; Razack, M. Hydrodynamic Characterization of Muğla Karst Aquifer Using Correlation and Spectral Analyses on the Rainfall and Springs Water-Level Time Series. *Water* **2019**, *12*, 85. [[CrossRef](#)]
53. Li, Y.; Liu, H.; Li, G.; Luo, W.; Sun, Y. Manure digestate storage under different conditions: Chemical characteristics and contaminant residuals. *Sci. Total Environ.* **2018**, *639*, 19–25. [[CrossRef](#)] [[PubMed](#)]
54. Appiah-Effah, E.; Duku, G.A.; Dwumfour-Asare, B.; Manu, I.; Nyarko, K.B. Toilet chemical additives and their effect on faecal sludge characteristics. *Heliyon* **2020**, *6*, e04998. [[CrossRef](#)] [[PubMed](#)]
55. Lee, C.L.; Chin, K.L.; H'ng, P.S.; Rashid, U.; Maminski, M.; Khoo, P.S. Effect of pretreatment conditions on the chemical-structural characteristics of coconut and palm kernel shell: A potentially valuable precursor for eco-efficient activated carbon production. *Environ. Technol. Innov.* **2020**. [[CrossRef](#)]
56. Santana, N.A.; Jacques, R.J.S.; Antonioli, Z.I.; Martínez-Cordeiro, H.; Domínguez, J. Changes in the chemical and biological characteristics of grape marc vermicompost during a two-year production period. *Appl. Soil Ecol.* **2020**, *154*, 103587. [[CrossRef](#)]
57. Chen, H.; Zhang, W.; Zhou, Y.; Li, J.; Zhao, H.; Xu, S.; Xia, W.; Cai, Z.; Li, Y. Characteristics of exposure to multiple environmental chemicals among pregnant women in Wuhan, China. *Sci. Total Environ.* **2021**, *754*, 142167. [[CrossRef](#)]
58. Li, T.; Liu, B.; Bi, X.; Wu, J.; Zhang, Y.; Feng, Y. Size and chemical characteristics of particles emitted from typical rural biomass cookstoves in North China. *Atmos. Res.* **2021**, *249*, 105295. [[CrossRef](#)]

59. Li, C.; Gao, X.; Wang, W.; Zhang, X.; Zhang, X.; Jiang, C.; Wang, Y. Hydro-biogeochemical processes of surface water leakage into groundwater in large scale karst water system: A case study at Jinci, northern China. *J. Hydrol.* **2020**. [[CrossRef](#)]
60. Valiente, N.; Gil-Márquez, J.M.; Gómez-Alday, J.J.; Andreo, B. Unraveling groundwater functioning and nitrate attenuation in evaporitic karst systems from southern Spain: An isotopic approach. *Appl. Geochem.* **2020**, *123*, 104820. [[CrossRef](#)]
61. Yue, F.J.; Li, S.L.; Waldron, S.; Wang, Z.J.; Oliver, D.M.; Chen, X.; Liu, C.-Q. Rainfall and conduit drainage combine to accelerate nitrate loss from a karst agroecosystem: Insights from stable isotope tracing and high-frequency nitrate sensing. *Water Res.* **2020**, *186*, 116388. [[CrossRef](#)]
62. Choi, B.Y.; Yun, S.T.; Mayer, B.; Hong, S.Y.; Kim, K.H.; Jo, H.-Y. Hydrogeochemical processes in clastic sedimentary rocks, South Korea: A natural analogue study of the role of dedolomitization in geologic carbon storage. *Chem. Geol.* **2012**, *306–307*, 103–113. [[CrossRef](#)]
63. Rameil, N. Early diagenetic dolomitization and dedolomitization of Late Jurassic and earliest Cretaceous platform carbonates: A case study from the Jura Mountains (NW Switzerland, E France). *Sediment. Geol.* **2008**, *212*, 70–85. [[CrossRef](#)]